Final Report Template

Project Title:	Perovskite Solar Cells: Addressing Low Cost, High Efficiency, and Reliability Through Novel Hole-Transport Materials
Project Period:	10/01/17 – 9/30/18
Project Budget:	$192,529 ($21,385 cost share)
Submission Date:	12/12/2018
Recipient:	Colorado School of Mines
Address:	1210 14th Street, Coolbaugh Hall Golden, CO 80401
Award Number:	DE-EE00008174
Project Team:	Sellinger Research Group
Principal Investigator:	Alan Sellinger, Associate Professor Chemistry, and Materials Science Phone: 303-382-2586 Email: aselli@mines.edu

Acknowledgment: "This material is based upon work supported by the Department of Energy under award number DE-EE00008174"

Disclaimer: "This report was prepared as an account of work sponsored by an agency of the United States Government. Neither the United States Government nor any agency thereof, nor any of their employees, makes any warranty, express or implied, or assumes any legal liability or responsibility for the accuracy, completeness, or usefulness of any information, apparatus, product, or process disclosed, or represents that its use would not infringe privately owned rights. Reference herein to any specific commercial product, process, or service by trade name, trademark, manufacturer, or otherwise does not necessarily constitute or imply its endorsement, recommendation, or favoring by the United States Government or any agency thereof. The views and opinions of authors expressed herein do not necessarily state or reflect those of the United States Government or any agency thereof."

Executive Summary: The ultimate goal of this project is to develop low-cost and scalable organic-based hole transport materials that will lead to thin film perovskite solar cells with high efficiencies (>25%) and long lifetimes (>20 years). A very important component of a perovskite solar cell is the hole transport layer (HTL). This layer is also generally the most expensive and problematic component of the device. Currently the state-of-the-art HTL is based on a lithium salt doped aromatic amine termed N^2,N^2,$N^{2'}$,$N^{2'}$,N^7,N^7,$N^{7'}$,$N^{7'}$-octakis(4-methoxyphenyl)-9,9′-spirobi[9H-fluorene]-2,2′,7,7′-tetramine **(**spiro-OMeTAD) that is very difficult to prepare with no paths for becoming cost effective at high volume. This project will directly prepare perovskite solar cells more easily commercialized by designing and preparing new HTL materials with properties that address the current bottlenecks, such as cost, tunable conductivity and energy levels, hydrophobicity, Li free dopants, and stability to name a few. We have preliminary results from new cost-effective HTLs and dopants that have led to high efficiency (>19%) and long operating lifetime devices without encapsulation – significantly improved over spiro-OMeTAD based devices prepared in our labs as controls. We will focus on using the lessons learned from that first departure from the norm to design even more ideal and scalable HTLs. We believe the outcomes of this proposal will lead to a substantial impact for the perovskite community to develop a low cost, scalable and high performing HTL. This will be a collaborative effort where our synthetic chemists will perform HTL design, chemical synthesis, and materials characterization, while our device engineers will perform device physics, fabrication/processing, and characterization.

Background:

Rapid power conversion efficiency (PCE) improvements from 3.83%[1] to 23.3%[2] in less than a decade, perovskite solar cells (PSCs) have great potential to serve as a low-cost, renewable electricity source to meet increasing energy demands. Even so, devices durable enough for real world power generation is needed prior to commercialization, which is significantly impacted by hole-transport layer (HTL) formulation.

Most organic-based HTLs for PSCs require dopants for improved charge-transport properties. The state-of-the-art organic hole-transport materials (HTMs) in PSCs, such as 2,2′,7,7′-tetrakis(*N,N*-di-*p*-methoxyphenylamine)-9,9′-spirobifluorene (*spiro-OMeTAD*) and poly(triarylamine) (*PTAA*), utilize bis(trifluoromethane)sulfonamide lithium salt (LiTFSI) as a dopant for improved fill factor (FF) and PCE.[3–5] In the prototypical case of spiro-OMeTAD, LiTFSI contributes to the formation of spiro-OMeTAD radical cations in the presence of oxygen,[6,7] which in turn promotes charge hopping[8–10] and increases the hole mobility and conductivity of the HTL. However, the radical cation generation is typically inconsistent, as it is not directly related to dopant concentration and very dependent on atmospheric exposure conditions.[6,11,12] While use of such dopants improves charge-transport properties to realize high PCE, the dopants can be detrimental to the overall stability of PSCs as the films need to be exposed to ambient oxygen, that of course introduces water. Additionally, the hygroscopic Li^+ cations have been shown to migrate through the entire device stack[13] increasing moisture ingress.[14,15]

In contrast to the non-stoichiometric *in situ* radical cation generation achieved with LiTFSI doping, an HTM's conductivity may also be increased by the addition of its oxidized salt analogue. Nguyen et al.[16] combined spiro-OMeTAD with its oxidized salt

doped analogue, 2,2′,7,7′-tetrakis(*N,N*-di-*p*-methoxyphenylamine)-9,9′-spirobifluorene di[bis(trifluoromethanesulfonyl)imide] (*spiro(TFSI)$_2$*) and demonstrated improved HTL conductivity and PSC PCE without use of hygroscopic lithium salts. Moreover, this strategy allows for precise control over doping concentrations, eliminates the need for oxygen exposure, and is also far less susceptible to unwanted ion intercalation in the active layer. Leijtens et al.[17,18] implemented this strategy with a low-cost, synthetically simple carbazole-cored HTM for comparable PCEs and improved hydrophobicity by using *EH44* (9-(2-ethylhexyl)-*N*^{2},*N*^{2},*N*^{7},*N*^{7}-tetrakis(4-methoxyphenyl)-9*H*-carbazole-2,7-diamine) doped with its analogue TFSI$^-$ radical cation salt, *EH44-ox* (9-(2-ethylhexyl)-*N*^{2},*N*^{2},*N*^{7},*N*^{7}-tetrakis(4-methoxyphenyl)-9*H*-carbazole-2,7-diamine bis(trifluoromethanesulfonyl)imide). With further device engineering by Christians et al.[19], unencapsulated PSCs utilizing EH44/EH44-ox as the HTL retained 88% average PCE over 1000 hours of continuous operation, dramatically outperforming LiTFSI-doped spiro-OMeTAD with respect to stability and lifetime. This report currently represents the highest stability unencapsulated perovskite solar cell measured in ambient conditions.

Despite these impressive findings with regard to PSC stability, PCEs suffer slightly using this HTL motif as compared to devices utilizing Li$^+$-doped spiro-OMeTAD. To this end, little is known about designing new HTMs that form stable cationic TFSI$^-$ salt doped analogues for efficient charge injection layers, as the few reports simply exchange the HTM core rather than the triarylamine pendant substituents that are directly involved in charge-transport.[20,16,18,21,22] Herein we report the synthesis of novel HTMs and their oxidized TFSI$^-$ salt analogues (HTM-ox) to assess PSC performance and lifetime as a function of both HTM and oxidized salt dopant, as well as present design criteria for preparing HTMs with stable doped analogues for efficient PSCs.

Introduction:

Our first task was to design and prepare HTM materials and their corresponding Li-free oxidized dopants, and fully characterize using the equipment/techniques described above. Go/no-go decision points would include unforeseen synthetic bottlenecks that result in low yield (<40%), and tedious purification (difficult column chromatography using significant amounts of solvents). Any HTL that requires this difficulty would be eliminated from consideration. Results will be disseminated through conference presentations and publications. We will prepare perovskite devices using the prepared HTL materials from Task 1 and compare with spiro-OMeTAD HTLs. Previous work on the HTL from Scheme 1 with R = OCH_3 provided a window of HTL thickness and doping that is greatly optimized over our first attempts. This task will replicate these studies with new HTLs to develop rough guidelines for HTLs that lead to optimized device performance for a variety of absorber layer configurations. The results from this task will directly affect what HTL materials will be prepared in Task 1. A go/no-go decision for working on a material will be: if a material is consistently performing poorly (< 80% of control) after device optimization, then it would be eliminated from further consideration in perovskite solar cell devices. Results will be disseminated through conference presentations and publications. Three new HTL materials (5g each) that outperform spiro-OMeTAD in terms of cost (we will provide a cost comparison to spiro-OMeTAD),

and performance. Demonstrate a 1cm^2 active area perovskite solar cell with a PCE >19% and 2.2X improvement in lifetime over spiro-OMeTAD based devices.

Project Results and Discussion:

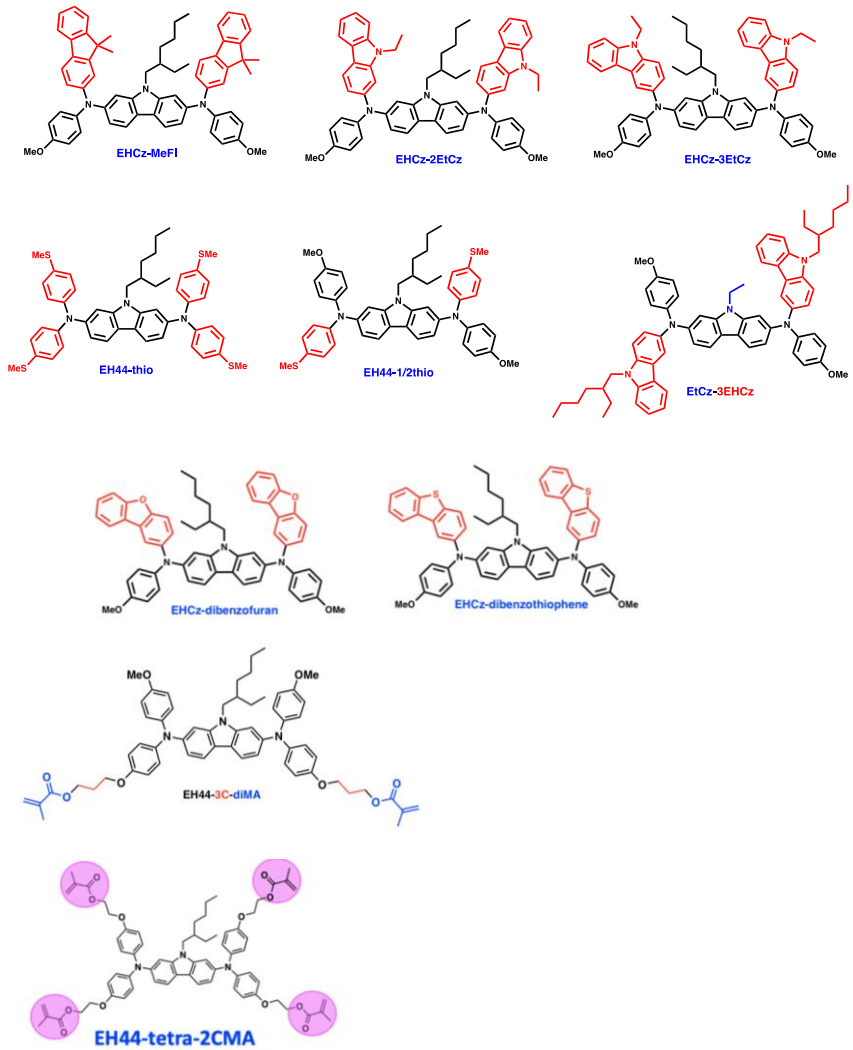

Figure 1: HTMs portfolio synthesized on the gram-level scale. Oxidized salts for dopants of each HTM have been synthesized on the 100 mg scale.

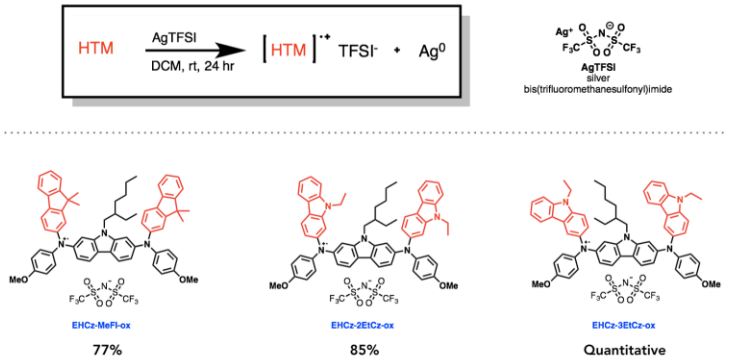

Scheme 1: Synthetic scheme for preparing oxidized salt dopants.

Ten novel HTMs, **Figure 1**, have been synthesized at scales of 100 mg or more and at least 20 mg of each corresponding oxidized HTM, used as a dopant, has been prepared. The optoelectronic and physical properties have been thoroughly characterized for each new HTM. Here, we will highlight results from three HTMs: EHCz-MeFl, EHCz-2EtCz, and EHCz-3EtCz. While maintaining proper energetic alignment with the perovskite, thermal properties of three new HTMs are superior to EH44 (**Table 1**). Additionally, oxidized salts for each HTM have been synthesized for use as lithium-free dopants in devices for high stability (**Scheme 1**).

Utilizing a FAMACS[23] active layer (**Figure 2**), PCEs are comparable among EH44 and EHCz-3EtCz, yet the latter affords higher open-circuit voltages, **Table 2**. Furthermore, performance of EHCz-MeFl and EHCz-2EtCz

Table 1: Thermal properties of pristine HTM - decomposition temperature (T_d) and glass transition temperature (T_g) [1]error is +/- 0.01 wt. % [2]error is +/- 0.1 ˚C

	$T_{d,\,onset}$ (˚C)[1]	T_g (˚C)[2]
EH44	349	69
EHCz-MeFl	393	100
EHCz-2EtCz	423	98
EHCz-3EtCz	397	99
EtCz-3EHCz	409	88
EHCz-DBT	424	97
EHCz-DBF	395	83
EHCz-3C-diMA	-	44

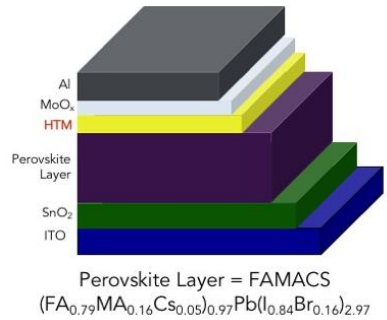

Figure 2: Device stack of perovskite solar cells prepared with novel HTMs.

Table 2: Preliminary optimized device performance of novel HTMs. Each HTM was processed under different conditions and average values from 5-10 devices are shown. EHCz-3EtCz was processed from a 25 mg/mL (total concentration) and 26 wt% EHCz-3EtCz preoxidized salt. EHCz-2EtCz was processed from a 20 mg/mL (total concentration) and 14wt% EH44 preoxidized salt. EHCz-MeFl was processed from a 15 mg/mL (total concentration) and 14wt% EH44 preoxidized salt.

HTM (Scan Direction)	J_{SC} (mA/cm^2)	V_{OC} (eV)	FF (%)	PCE (%)
EHCz-3EtCz (Rev)	20.82	1.09	67.50	15.35
EHCz-3EtCz (Fwd)	20.92	1.07	68.99	15.50
EHCz-2EtCz (Rev)	20.89	1.08	66.75	15.01
EHCz-2EtCz (Fwd)	20.86	1.05	67.34	14.73
EHCz-MeFl (Rev)	20.84	1.03	60.96	13.15
EHCz-MeFl (Fwd)	20.69	1.00	58.80	12.25

* (Reference Devices: Spiro Rev = 16.91%, Fwd = 15.91%, and EH44 Rev = 15.53%, Fwd = 15.10%)

were significantly improved with use of EH44-ox as dopant instead of their analogous oxidized salt dopant (EHCz-MeFl-ox and EHCz-2EtCz-ox respectively).

To elucidate mechanism(s) for performance differences, both solution-phase (UV-Vis absorption) and solid-state characterization of the HTMs were investigated (energy level energetics, charge conductivity and mobility). For all HTMs except EHCz-3EtCz, dopant addition reduced the E_{HOMO} (**Table 3**). Therefore, energetic alignment with the valence band of the perovskite cannot explain performance differences. UV-Vis absorption spectroscopy assessed stability of HTM + 14 wt.% oxidized salt dopant, as the oxidized salt has a characteristic absorption band around 450nm to 550nm. For EH44 and EH44-ox and EHCz-3EtCz and EHCz-3EtCz-ox, the dopant absorption is observed when mixing pristine HTM with its oxidized salt. Although, for EHCz-MeFl and EHCz-2EtCz, their respective dopants are not observable when mixed with pristine HTM. We can conclude that the para oxygen or nitrogen in EH44-ox and EHCz-3EtCz-ox respectively stabilized the radical cation dopant, whereas the para carbon and meta nitrogen in EHCz-2EtCz-ox and EHCz-MeFl are not a strong enough electron donating group and therefore cannot stabilize the radical cation. Matrix Assisted Laser Desorption Ionization Mass Spectrometry (MALDI MS) suggests dopant dimerization to possibly explain the macroscopic observations. These findings allow us to simplify further device fabrication, as stable oxidized salt dopants like EH44-ox can be used for any HTL, as opposed to unique oxidized salts for each new HTL.

Table 3: Photoemission spectroscopy in air (PESA) data for new neat HTMs along with 14 wt.% pre-oxidized salts

Sample	E_{HOMO}(eV)
spiro + tbp	5.10
spiro doped + LiTFSI + tbp	5.32
EH44 + tbp	5.10
EH44 + EH44-ox + tbp	5.20
EHCz-3EHCz + tbp	5.01
EHCz-3EHCz + EHCz-3EHCz-ox + tbp	5.02
EHCz-3EHCz + EH44-ox + tbp	5.03
EHCz-2EtCz + tbp	5.05
EHCz-2EtCz + EHCz-2EHCz-ox + tbp	5.13
EHCz-2EtCz + EH44-ox + tbp	5.15
EHCz-MeFl + tbp	5.13
EHCz-MeFl + EHCz-MeFl-ox + tbp	5.20
EHCz-MeFl + EH44-ox + tbp	5.20

PESA experiments performed on drop cast thin films on glass slides by Chuck Hitzman, Director Surface Analysis Lab, Stanford University Nano Shared Facility.

Table 4: Summary of HTM hole mobility values measured by SCLC

	Hole Mobility (10^{-5} cm^2/Vs)
Spiro Not Doped	0.36
Spiro + LiTFSI	17.20
EH44 Not Doped	1.66
EH44 + EH44-ox	10.60
EHCz-3EtCz Not Doped	0.78
EHCz-3EtCz + EHCz-3EtCz-ox	0.87
EHCz-3EtCz + EH44-ox	1.09
EHCz-2EtCz Not Doped	0.50
EHCz-2EtCz + EHCz-2EtCz-ox	1.16
EHCz-2EtCz + EH44-ox	10.70
EHCz-MeFl Not Doped	0.23
EHCz-MeFl + EHCz-MeFl-ox	0.21
EHCz-MeFl + EH44-ox	2.81
EHCz-MeFl + EH44-ox	2.07

The hole mobility of these new HTMs was measured using space-charged limited current (SCLC), as shown in **Table 4**. The HTMs with higher hole-mobility have a higher FF and PCE, which correlates well with literature. Additionally, mobility correlates with dopant stability described above.

New HTMs outperform EH44 and spiro-OMeTAD control devices at both 50 and 70 ºC. At 50 ºC, all three new HTMs maintain at least 60% PCE after 500 hours of *unencapsulated*, continuous operation (**Figure 4**). Stabilized power outputs (SPO) of EHCz-3EtCz at before again are on par with Li-doped Spiro-OMeTAD, and EHCz-MeFl and EHCz-2EtCz are on par with EH44. At 70 ºC, higher glass transition (T_g) materials EHCz-3EtCz, -2EtCz, and -MeFl all function at the end of the 500 hours of unencapsulated, continuous operation, and EHCz-2EtCz and -MeFl maintain at least 50% of initial PCE. While pristine glass transition temperature (T_g) are identical for the three new HTMs, we observe different thermal behavior from the mixed HTLs, as EHCz-3EtCz, the highest performing HTM in the series at 50 ºC suffers at 70 ºC. Spiro-OMeTAD + LiTFSI and Spiro + Spiro-OMeTAD-ox suffer severe degradation over the first 100 hours and stop working by 300 hours.

Further stability testing has been performed to understand the mechanisms of degradation, especially at higher temperatures. The device stability of each new HTM

(a)

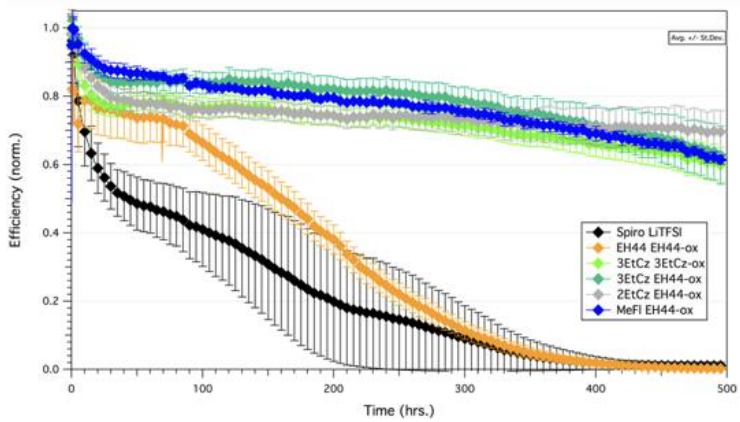

	SPO Before	SPO After
Spiro LiTFSI	16.06, 16.58, 16.44	0, 0, 0
EH44 EH44-ox	14.50, 14.82, 14.80	0, 0, 3.30
3EtCz 3EtCz-ox	16.05, 15.61, 15.77	10.21, 9.07, 8.46
3EtCz EH44-ox	16.01, 16.04, 15.81	10.78, 9.32, 8.52
2EtCz EH44-ox	14.61, 12.97, 15.00	9.58, 9.41, 9.49
MeFl EH44-ox	14.27, 13.54	7.66, 7.63

(b)

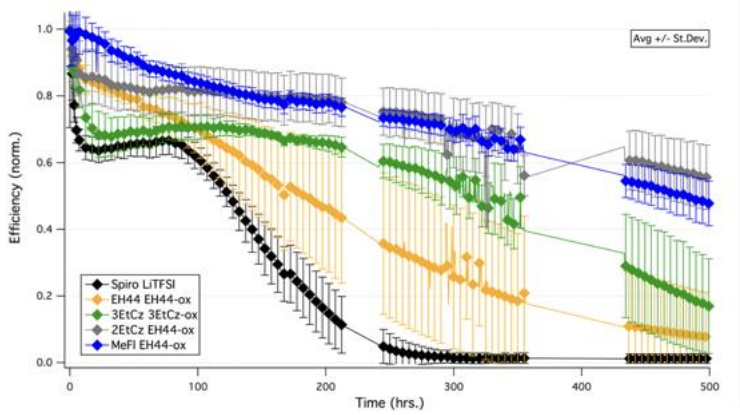

	SPO Before	SPO After
Spiro LiTFSI	16.78, 16.51, 16.65	0.01, 0.001, 0.0003
EH44 EH44-ox	14.69, 15.20	0.31, 0.25
3EtCz 3EtCz-ox	16.01, 16.14, 15.77	0.20, 0.49, 4.71
2EtCz EH44-ox	14.46, 14.56, 14.86	5.93, 7.22, 7.60
MeFl EH44-ox	12.58, 12.57, 12.11	5.71, 6.31, 5.22

Figure 4: 500 hour stability assessment of unencapsulated devices at 50 ºC (a) and 70 ºC (b). The graphs show normalized efficiencies, and the tables show stabilized power outputs (SPO).

and Spiro-OMeTAD, as a control, was measured for devices tested at 70°C under nitrogen (thus the absence of oxygen and water). These results were then compared with the device stability data at 70°C under ambient conditions (with oxygen and water) for each HTM. For ease of understanding in **Figure 5** we only compare the stability of Spiro-OMeTAD and EHCz-2EtCz at 70°C under both a nitrogen atmosphere and ambient atmosphere. Spiro-OMeTAD under ambient conditions has a large initial drop in performance, burn-in, and eventually drops to zero within 250hrs. Under nitrogen Spiro-OMeTAD still has an initial drop in performance followed by a slower decay component. Whereas, EHCz-2EtCz has very similar performance decay whether it is under nitrogen or ambient conditions. We see a very similar trend for EHCz-3EtCz and EHCz-MeFl. This could indicate that the HTM is thermally stable, although, another part of the device stack may not be thermally stable at these high temperatures. Most of the performance drop for EHCz-2EtCz is related to a drop in the fill factor (FF) from an increase in the series resistance over time. Literature indicates that this could be due to instabilities in the MoO_3 interlayer over time under high temperatures. Therefore, we are currently testing this hypothesis in attempt in improve the thermal stability even more.

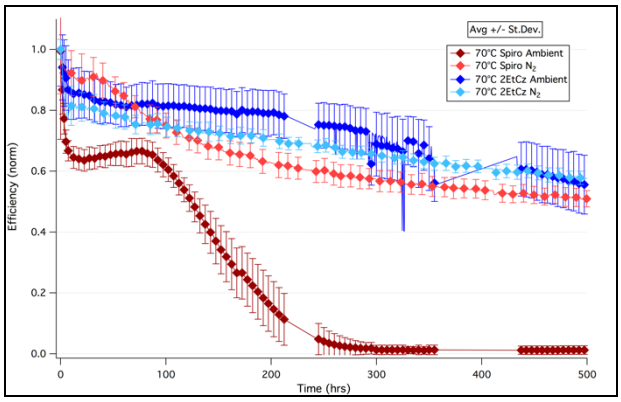

Figure 5: Comparing the normalized device performance, using Spiro-OMeTAD or EHCz-2EtCz as the HTM, unencapsulated with constant heating at 70°C and constant illumination for 500 hrs.

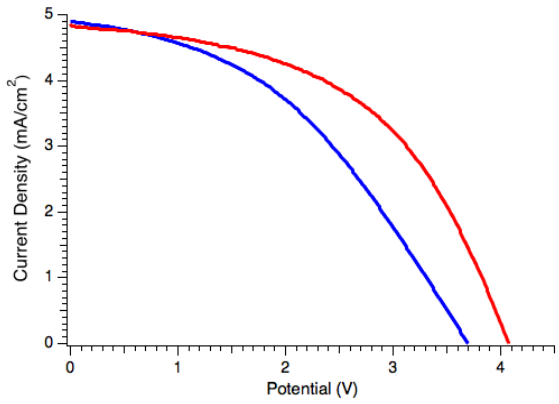

Figure 6: JV curves for mini-modules with spiro-OMeTAD (red) and EHCz-3EtCz (blue) as HTL.

Table 5: Summary of energetic characterization. Optical bandgap were derived from absorption onset, E_{HOMO} were derived from thin-film cyclic voltammetry, and E_{LUMO} were calculated using $E_{gap,onset}=E_{LUMO}-E_{HOMO}$.

	$E_{gap,\ onset}$ (eV)	E_{HOMO} (ev)	E_{LUMO} (eV)
EtCz-3EHCz	2.88	-4.67	-1.79
EHCz-DBT	2.94	-4.83	-1.89
EHCz-DBF	2.93	-4.90	-1.97

EHCz-3EtCz, the most promising HTM, was integrated into a mini-module and compared to a mini-module with Li-doped spiro-OMeTAD as a control. The device stack is shown in **Figure 2**. In **Figure 6**, we show the JV curves for four cells connected in series with a device area of 7.84 cm^2. Device with spiro-OMeTAD-based HTL generated a PCE=9.89%, FF=50.0%, Jsc = 4.86 mA/cm2, Voc = 4.07 V, and a geometric FF of 90%. Device with EHCz-3EtCz as HTL generated a PCE=7.51%, FF=41.4%, Jsc = 4.90 mA/cm^2, Voc = 3.69 V, and a geometric FF of 90%. This is impressive, especially since the typical device area of test cells is 0.058 cm^2. We look forward to optimizing these mini-modules for stable electricity generation *via* PSC with stable charge-transport layers.

EHCz-3EtCz provided highest device efficiencies as compared to the other new HTMs previously discussed. Thus, we designed new HTMs (EtCz-3EHCz, EHCz-DBF, and EHCz-DBT) to understand why this has superior performance to further improve performance (**Figure 1**). EtCz-3EHCz was used to probe importance of HTL morphology, as it is identical to EHCz-3EtCz except for the placement of solubilizing alkyl chains. To better understand the importance of the extended conjugation network attached to the triarylamine (*i.e,* methoxyphenyl groups on EH44 versus carbazole and methoxyphenyl groups on EHCz-3EtCz), we replaced the nitrogen on the carbazole with sulfur and oxygen respectively. Finally, cross-linkable groups were attached in EH44-3C-diMA to further improve device thermal stability by locking in HTL morphology after cross-linking. The optoelectronic and physical properties have been thoroughly characterized for each new HTM, and are appropriate for device integration with respect to energetic alignment and high thermal stability (**Table 1**, **Table 5**).

The initial performance of the HTMs are summarized herein. EtCz-3EHCz as hole-transport layer (HTL) resulted in similar PCE as EHCz-3EtCz. This points to minimal change in charge-transport properties with different steric demands (*i.e.*, change in alkyl chain position). With regard to EHCz-dibenzofuran and EHCz-dibenzothiophene as HTL, devices showed low PCE and FF, which we found is likely due to low HTL hole mobility.

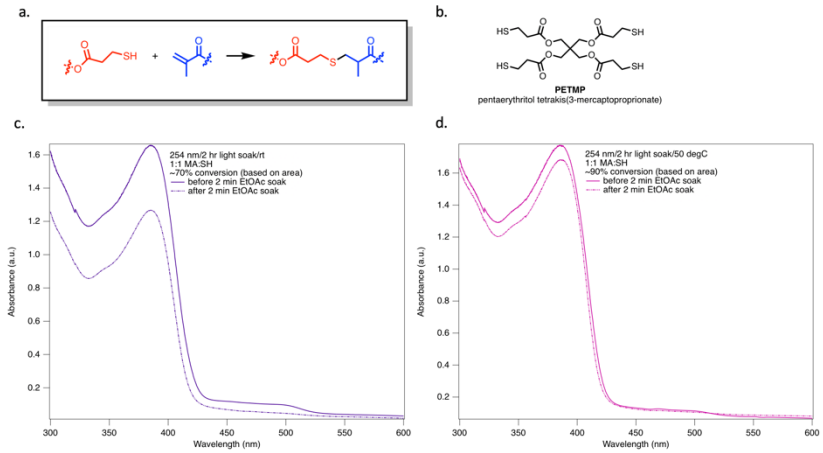

Figure 7: (a) Scheme depicting initiator-free crosslinking of a thiol with methacrylate (b) chemical structure of PETMP, the crosslinker used in this study, UV-Vis absorption spectra of HTM + PETMP in a 1:1 methacrylate: thiol stoichiometry before and after crosslinking (254 nm, 2 hr)/solvent soak. Irradiation at room temperature (c) and 50 ºC (d).

Designing a cross-linkable HTM is challenging as the cross-linking agent has been shown to be damaging to the perovskite active layer.[24] Moreover, eliminating additional additives in the HTL is desired for simple fabrication, therefore, we decided to pursue initiator-free methods for HTL polymerization or crosslinking for improved HTL thermal stability and solvent resistance. While EH44-3C-diMA does not polymerize upon heat nor irradiation, it can be crosslinked in the presence of an inexpensive crosslinker pentaerythirtol tetrakis(3-mercaptopropionate (PETMP) (**Figure 7a-b**). From UV-Vis absorption spectra, we see improved solvent resistance after 2 hrs of 254 nm irradiation (**Figure 7c-d**, room temperature and 50 ºC). However, initial device application has not led to high performance. This is likely due to the extended time the device must be irradiated at 254 nm.

To reduce HTM glass transition temperature, and thus cross-linking time, we synthesized a tetra-crosslinkable HTM, EH44-tetra-2CMA (**Figure 8**). In addition to cross-linking time, another obstacle with regard to integrating cross-linkable HTM in PSC stack is that they still require doping for optimal charge-transport properties and PSC performance. The concern is that during the free-radical cross-linking process

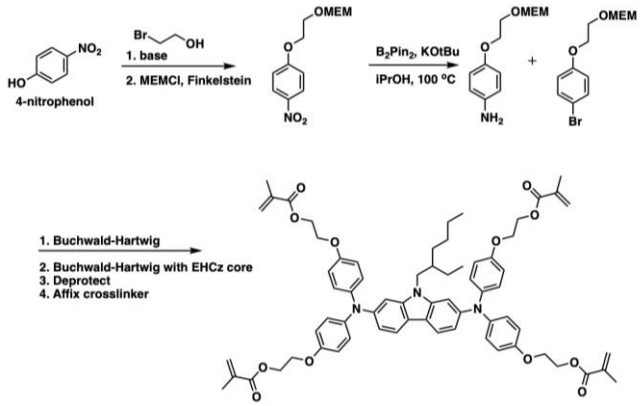

Figure 8: EH44 and EH44-tetra-2CMA (((((9-(2-ethylhexyl)-9*H*-carbazole-2,7-diyl)bis(azanetriyl))tetrakis(benzene-4,1-diyl))tetrakis(oxy))tetrakis(ethane-2,1-diyl) tetrakis(2-methylacrylate.

the dopant, a radical cation, may be reduced during this process and render the dopant ineffective. To assess this, we performed UV-Vis absorption spectroscopy to monitor the dopant's characteristic radical triarylamine absorption peak (500 nm) in the presence of the cross-linkable HTM and crosslinker. In **Figure 9**, we show that the radical triarylamine peak in the dopant remains stable in the presence of EH44-tetra-2CMA over 20 min. After addition of the crosslinker, PETMP (pentaerythirtol tetrakis(3-mercaptopropionate)) and irradiation at 254 nm the radical triarylamine peak remains stable. Thus, upon PSC integration, we predict that this system will remain appropriately doped for well-performing devices.

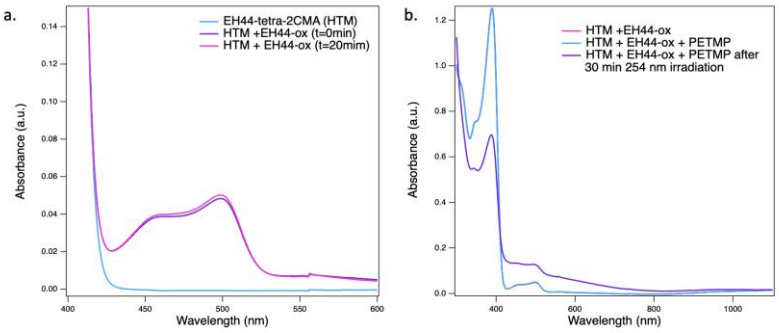

Figure 9: UV-Vis Absorption spectra of EH44-tetra-2CMA in presence of EH44-ox (a) and EH44-tetra-2CMA and EH44-ox in presence of PETMP before and after 254 nm irradiation (b).

Conclusions: All milestones have been achieved in the anticipated timeframe. Two high impact publications are in peer review, the first with regard to dopant design and preliminary stability results, and the second a review on HTL dopants for PSC. All final project deliverables are met with the exception of the >19% efficiency for >1cm^2 active area. Device with spiro-OMeTAD-based HTL generated a PCE=9.89%, FF=50.0%, Jsc = 4.86 mA/cm2, Voc = 4.073 V, and a geometric FF of 90%. Device with EHCz-3EtCz as HTL generated a PCE=7.51%, FF=41.42%, Jsc = 4.90 mA/cm^2, Voc = 3.697 V, and a geometric FF of 90%. This is impressive, especially since the typical device area of test cells is 0.058 cm^2.

Path Forward:

We are completing work towards the publication of full scope PSC stability utilizing novel HTL formulations on the mini-module scale. Furthermore we are working with other research groups and small companies to evaluate our materials for use in commercial devices. Lastly we believe our HTMs will be very important for future technology involving tandem solar cells.

Publications Resulting from This Work:

1. "Doping Strategies for Small Molecule Organic Hole-Transport Materials: Impacts on Perovskite Solar Cell Performance and Stability" T.H. Schloemer, J.A. Christians, J.M. Luther, A. Sellinger. *Accepted, Chemical Science,* **2019**
2. "Design Criteria for Preparing Lithium-Free Doped Organic Small Molecule Hole-Transport Layers in Perovskite Solar Cells with Enhanced Thermal Stability" T. H. Schloemer, Timothy S. Gehan, Jeffrey A. Christians, Deborah G. Mitchell, Alex Dixon, Zhen Li, Kai Zhu, Joseph J. Berry, Joseph M. Luther, and Alan

Sellinger. *ACS Energy Letters,* **2019***,* https://pubs.acs.org/doi/10.1021/acsenergylett.8b02431

3. "Achieving High Thermal Stability of Perovskite Solar Cells" Timothy S. Gehan, T. H. Schloemer, Jeffrey A. Christians, Kai Zhu, Joseph J. Berry, Joseph M. Luther, and Alan Sellinger. *In Preparation.*

References:

(1) Kojima, A.; Teshima, K.; Shirai, Y.; Miyasaka, T. Organometal Halide Perovskites as Visible-Light Sensitizers for Photovoltaic Cells. *J. Am. Chem. Soc.* **2009**, *131* (17), 6050–6051. https://doi.org/10.1021/ja809598r.

(2) NREL Photovoltaic Efficiency Chart. https://www.nrel.gov/pv/assets/images/efficiency-chart.png.

(3) Ko, Y.; Kim, Y.; Lee, C.; Kim, Y.; Jun, Y. Investigation of Hole-Transporting Poly(Triarylamine) (PTAA) on Aggregation and Charge Transport for Hysteresis-Less Scalable Planar Perovskite Solar Cells. *ACS Appl. Mater. Interfaces* **2018**. https://doi.org/10.1021/acsami.7b18745.

(4) Hawash, Z.; Ono, L. K.; Qi, Y. Recent Advances in Spiro-MeOTAD Hole Transport Material and Its Applications in Organic-Inorganic Halide Perovskite Solar Cells. *Adv. Mater. Interfaces* **2018**, *5* (1), 1700623. https://doi.org/10.1002/admi.201700623.

(5) Jeon, N. J.; Na, H.; Jung, E. H.; Yang, T.-Y.; Lee, Y. G.; Kim, G.; Shin, H.-W.; Seok, S. I.; Lee, J.; Seo, J. A Fluorene-Terminated Hole-Transporting Material for Highly Efficient and Stable Perovskite Solar Cells. *Nat. Energy* **2018**, *3* (8), 682–689. https://doi.org/10.1038/s41560-018-0200-6.

(6) Abate, A.; Leijtens, T.; Pathak, S.; Teuscher, J.; Avolio, R.; E. Errico, M.; Kirkpatrik, J.; M. Ball, J.; Docampo, P.; McPherson, I.; et al. Lithium Salts as "Redox Active" p-Type Dopants for Organic Semiconductors and Their Impact in Solid-State Dye -Sensitized Solar Cells. *Phys. Chem. Chem. Phys.* **2013**, *15* (7), 2572–2579. https://doi.org/10.1039/C2CP44397J.

(7) Namatame, M.; Yabusaki, M.; Watanabe, T.; Ogomi, Y.; Hayase, S.; Marumoto, K. Direct Observation of Dramatically Enhanced Hole Formation in a Perovskite-Solar-Cell Material Spiro-OMeTAD by Li-TFSI Doping. *Appl. Phys. Lett.* **2017**, *110* (12), 123904. https://doi.org/10.1063/1.4977789.

(8) Walzer, K.; Maennig, B.; Pfeiffer, M.; Leo, K. Highly Efficient Organic Devices Based on Electrically Doped Transport Layers. *Chem. Rev.* **2007**, *107* (4), 1233–1271. https://doi.org/10.1021/cr050156n.

(9) Lüssem B.; Riede M.; Leo K. Doping of Organic Semiconductors. *Phys. Status Solidi A* **2012**, *210* (1), 9–43. https://doi.org/10.1002/pssa.201228310.

(10) Lüssem, B.; Keum, C.-M.; Kasemann, D.; Naab, B.; Bao, Z.; Leo, K. Doped Organic Transistors. *Chem. Rev.* **2016**, *116* (22), 13714–13751. https://doi.org/10.1021/acs.chemrev.6b00329.

(11) Snaith, H. J.; Grätzel, M. Enhanced Charge Mobility in a Molecular Hole Transporter via Addition of Redox Inactive Ionic Dopant: Implication to Dye-

Sensitized Solar Cells. *Appl. Phys. Lett.* **2006**, *89* (26), 262114. https://doi.org/10.1063/1.2424552.

(12) Schölin, R.; Karlsson, M. H.; Eriksson, S. K.; Siegbahn, H.; Johansson, E. M. J.; Rensmo, H. Energy Level Shifts in Spiro-OMeTAD Molecular Thin Films When Adding Li-TFSI. *J. Phys. Chem. C* **2012**, *116* (50), 26300–26305. https://doi.org/10.1021/jp306433g.

(13) Li, Z.; Xiao, C.; Yang, Y.; Harvey, S. P.; Kim, D. H.; Christians, J. A.; Yang, M.; Schulz, P.; Nanayakkara, S. U.; Jiang, C.-S.; et al. Extrinsic Ion Migration in Perovskite Solar Cells. *Energy Env. Sci* **2017**, *10*, 1234–1242. https://doi.org/10.1039/C7EE00358G.

(14) Hawash, Z.; Ono, L. K.; Raga, S. R.; Lee, M. V.; Qi, Y. Air-Exposure Induced Dopant Redistribution and Energy Level Shifts in Spin-Coated Spiro-MeOTAD Films. *Chem. Mater.* **2015**, *27* (2), 562–569. https://doi.org/10.1021/cm504022q.

(15) Christians, J. A.; Miranda Herrera, P. A.; Kamat, P. V. Transformation of the Excited State and Photovoltaic Efficiency of CH3NH3PbI3 Perovskite upon Controlled Exposure to Humidified Air. *J. Am. Chem. Soc.* **2015**, *137* (4), 1530–1538. https://doi.org/10.1021/ja511132a.

(16) Nguyen, W. H.; Bailie, C. D.; Unger, E. L.; McGehee, M. D. Enhancing the Hole-Conductivity of Spiro-OMeTAD without Oxygen or Lithium Salts by Using Spiro(TFSI)2 in Perovskite and Dye-Sensitized Solar Cells. *J. Am. Chem. Soc.* **2014**, *136* (31), 10996–11001. https://doi.org/10.1021/ja504539w.

(17) Snaith, H., Leijtens, T., Abate, A., Sellinger, A. Organic Semiconductor Doping Process. US 9,818,944 B4, November 14, 2017.

(18) Leijtens, T.; Giovenzana, T.; Habisreutinger, S. N.; Tinkham, J. S.; Noel, N. K.; Kamino, B. A.; Sadoughi, G.; Sellinger, A.; Snaith, H. J. Hydrophobic Organic Hole Transporters for Improved Moisture Resistance in Metal Halide Perovskite Solar Cells. *ACS Appl. Mater. Interfaces* **2016**, *8* (9), 5981–5989. https://doi.org/10.1021/acsami.5b10093.

(19) Christians, J. A.; Schulz, P.; Tinkham, J. S.; Schloemer, T. H.; Harvey, S. P.; Villers, B. J. T. de; Sellinger, A.; Berry, J. J.; Luther, J. M. Tailored Interfaces of Unencapsulated Perovskite Solar Cells for >1,000 Hour Operational Stability. *Nat. Energy* **2018**, *3* (1), 68. https://doi.org/10.1038/s41560-017-0067-y.

(20) Hsieh, B.; Li, X.C.; Sellinger, A. Semiconducting Hole Injection Materials for Organic Light Emitting Devices. U.S. Patent No. 6,830,830, December 4, 2004.

(21) Kasparavicius, E.; Magomedov, A.; Malinauskas, T.; Getautis, V. Long-Term Stability of the Oxidized Hole Transporting Materials Used in Perovskite Solar Cells. *Chem. - Eur. J.* **2018**, *24* (99), 9910–9918. https://doi.org/10.1002/chem.201801441.

(22) Qu, J.; Jiang, X.; Yu, Z.; Lai, J.; Zhao, Y.; Hu, M.; Yang, X.; Sun, L. Improved Performance and Air Stability of Perovskite Solar Cells Based on Low-Cost Organic Hole-Transporting Material X60 by Incorporating Its Dicationic Salt. *Sci. China Chem.* **2018**, *61* (2), 172–179. https://doi.org/10.1007/s11426-017-9141-9.

(23) Christians, J. A.; Schulz, P.; Tinkham, J.; Schloemer, T. H.; Harvey, S. P.; Tremolet de Villers, B.; Sellinger, A.; Berry, J. J.; Luther, J. M. Tailored Interfaces

of Unencapsulated Perovskite Solar Cells for >1000 Hours of Ambient Operational Stability. *Nat. Energy* **2017**, *Accepted*.

(24) Xu, J.; Voznyy, O.; Comin, R.; Gong, X.; Walters, G.; Liu, M.; Kanjanaboos, P.; Lan, X.; Sargent, E. H. Crosslinked Remote-Doped Hole-Extracting Contacts Enhance Stability under Accelerated Lifetime Testing in Perovskite Solar Cells. *Adv. Mater.* **2016**, *28* (14), 2807–2815. https://doi.org/10.1002/adma.201505630.